Fusion under a complex barrier

Basudeb Sahu
Department of Physics, Ravenshaw College, Cuttack-753 003, India

I. Jamir, E. F. P. Lyngdoh, and C. S. Shastry
Department of Physics, North Eastern Hill University, Shillong-793 022, India

(Received 22 July 1997)

The mechanism of fusion of two heavy nuclei is formulated within the concept of transmission across a mildly absorptive effective fusion barrier (EFB). The intensity of transmitted waves across such a barrier could be represented by the product $T_R P_S$ where T_R stands for the transmission coefficient across the corresponding real barrier and P_S is a factor of survival probability against absorption under the complex barrier. The justification of this result and the physical basis of the above EFB transmission model of fusion, which is complementary to the definition of fusion based on absorption in the interior region known as the direct reaction model (DRM), are demonstrated in the case of a complex square well potential with a complex rectangular barrier. Based on a WKB approach, expressions for T_R for different partial waves utilizing a realistic nucleus-nucleus potential are derived. Using the resulting expressions for the fusion cross section (σ_F), the experimental values of σ_F and the corresponding data of the average angular momentum of the fused body are explained satisfactorily over a wide range of energy around the Coulomb barrier in various heavy ion systems such as $^{16}O+^{152,154}Sm$, $^{58,64}Ni+^{58,64}Ni$, $^{64}Ni+^{92}Zr$, and $^{64}Ni+^{100}Mo$. [S0556-2813(98)05103-6]

PACS number(s): 25.70.Jj

I. INTRODUCTION

The magnitude and energy as well as angular momentum dependence of a heavy ion fusion cross section (σ_F) around Coulomb barrier energies has been a topic of renewed interest in recent times. Measured results of σ_F in the subbarrier region of energies are reported to be substantially larger than the values predicted by simple barrier penetration model calculations. Most of the improved theoretical approaches, though successful in analyzing the energy dependence of σ_F, fail to give a satisfactory explanation of the corresponding experimental spin distribution along with average angular momenta related to the fusion cross section. However, out of these approaches the coupled channel (CC) calculation, though tedious, is found to be more suited for the analysis of heavy ion (HI) reactions, barring some nearly symmetric pairs. The coupling of the relative motion of the two interacting nuclei to their excited states is believed to enhance the fusion cross section. This coupling of different channels like the excitation of collective degrees of freedom and transfer of nucleons on the elastic channel can be collectively represented by a complex polarization potential [1]. The imaginary part of this potential generated under a real potential barrier plays a significant role in the dynamics of the fusion process at energies around the Coulomb barrier. On the other hand, it has been predicted [2,3] that the channel couplings drastically change the shape of the conventional folding model potential, resulting in a sharp and strongly attractive real effective potential. Normally, one assumes that absorption into a compound nucleus does not occur until the whole of the real potential barrier obtained from folding model calculations has been traversed. This assumption of a local one-dimensional real potential with absorption into the fusion channel restricted to the region much interior to the barrier-peak position R_B is not adequate [4]. In view of the above facts, a more general one-dimensional potential theory for the analysis of HI fusion would utilize a complex local potential which allows absorption under an effective barrier that is expected to be thinner than the conventional one. One expects that the absorption builds up gradually from larger radii as the two densities of the interacting nuclei begin to overlap [5]. The extension of the absorption region until the barrier or beyond has been incorporated in the estimate of the absorption cross section for ion-ion reactions in Refs. [1,6–8]. In particular, the direct reaction model (DRM) of Udagawa *et al.* [8] visualizes that the imaginary part of the total optical model potential (OMP) can be divided into two parts. The reaction cross section generated by the inner part is recognized as the fusion cross section and the outer part represents other direct reactions or peripheral processes not proceeding towards compound nucleus formation. Thus, although the absorption has started building up from outside the Coulomb barrier, the amount of absorption from near the barrier-peak position inward is to be recognized as the fusion cross section and the absorption in the outer region may represent peripheral processes.

We can then visualize that fusion sets in after the system completes traversal of the mildly absorptive outer barrier region where direct or inelastic processes are effective and estimate the cross section for fusion by the formula

$$\sigma_F = \frac{\pi}{k^2} T_C, \tag{1}$$

where T_C indicates the intensity of transmitted waves for the complex effective fusion barrier. The symbol $k = (2\mu E_{\text{c.m.}}/\hbar^2)^{1/2}$ denotes the wave number, and μ is the reduced mass of the colliding system. Thus σ_F can be estimated from two different but complementary pictures: (i) from the absorption in the interior region $(0-R_F)$, where R_F

stands for the fusion radius parameter, and (ii) from the probability of reaching the radial distance R_F near R_B as a result of transmission from the outer region. The former method is known as the DRM of fusion [8] and the latter is termed as effective fusion barrier (EFB) transmission model by us [9–11]. In our previous calculations [9–11], we have assumed the barrier to be real and sharply falling in the interior side, consistent with the findings presented in Refs. [2,3]. The two approaches referred to here are capable of describing σ_F quite satisfactorily. Interestingly, the parameters R_F characterizing the onset of fusion in these two approaches lie very close to each other. This makes it desirable to demonstrate the complementary nature of these two models more explicitly. This requires the estimation of absorption from the region 0 to R_F and the transmission coefficient into this region, $r<R_F$, in the case of a complex barrier. We demonstrate the fact that the results of cross section from the DRM idea and EFB transmission concept incorporating absorption under the barrier are comparable by analyzing a complex square well potential followed by a complex rectangular barrier before we estimate σ_F for a realistic nucleus-nucleus system.

In order to make the EFB approach more sound and complete, we explicitly take into account the influence of the imaginary part $[W(r)]$ of the OMP in the process of transmission across the barrier. Adopting the mathematical procedure based on the WKB approximation [12], the transmission coefficient denoted by T_R for a given partial wave l will be derived semiclassically for an effective real potential generated by the real part of the OMP in the surface region. The effect of $W(r)$ in the surface region on the transmission process is represented by a multiplying factor (P_S) representing probability for survival against surface absorption and it is expressed as [13,14]

$$P_S=\exp\left[-\frac{2}{\hbar}\int_{R_F}^{\infty}\frac{W(r)}{v(r)}\,dr\right], \tag{2}$$

where $v(r)$ indicates the local velocity. This expression clearly shows that there is a decrease of probability of stay in the elastic channel with an increase of time of transit (τ_S) across the surface part of the real potential barrier. When τ_S increases more and more, the flux goes to inelastic or direct reaction channels. The factor P_S is the survival probability or a measure of no destruction after a period τ_S. Therefore, $(1-P_S)$ represents the factor for absorption to other channels. Thus the actual flux reaching a point R_F through a complex potential can be represented by the product $T_R P_S$, where T_R and τ_S are calculated along the real orbit specified by a certain l. Hence, replacing T_C by $T_R P_S$ in Eq. (1), σ_F can be calculated. As a result of this, one can avoid the use of complex turning points in the WKB approach adopted in the study of nucleus-nucleus reactions. The above concept, in turn, is related to the fact that due to a longer time of interaction and a larger value of $W(r)$ in the region $r<R_B$ the amplitude of absorption $(1-P_S)$ in this interior region is close to unity. In view of this we believe that whatever flux reaches the point $R_F\sim R_B$ will be totally absorbed, leading to complete fusion. The justification of splitting T_C into $T_R P_S$ is demonstrated in the case of a complex square barrier before going to the analysis of realistic nucleus-nucleus reactions.

We apply the present formulation, termed as modified WKB (MWKB) method, to the simultaneous analysis of experimental data for σ_F and the corresponding average angular momenta $(\langle l\rangle)$ of the compound nucleus in the case of several HI systems. In recent times, a great body of experimental data of these quantities for various pairs of nuclei over a wide range of energy around the Coulomb barrier is found in the literature. For our present study, we have selected three categories of systems such as (i) asymmetric (^{16}O+^{152,154}Sm), (ii) symmetric (^{58,64}Ni+^{58,64}Ni), and (iii) nearly symmetric (^{64}Ni+^{92}Zr and ^{64}Ni+^{100}Mo) pairs. Most of these systems have been studied successfully within the framework of the DRM [8] and EFB model using a real barrier [9,11]. On the other hand, the CC calculation is successful in the cases of systems under the first two categories, but not so good in the cases of the third category [18]. The success in analyzing the fusion data of all the above systems through the present formulation involving a complex barrier would show how our model is complementary to the DRM on the one hand and as good as and/or sometimes better than the most complicated CC calculations on the other.

In Sec. II, we give analytical expressions for a regionwise absorption in the case of a complex square well potential. The results of the reaction cross section in the interior region are compared with the values of the cross section estimated from transmission through a complex barrier and the complementary nature of the DRM and EFB concepts is established. In Sec. III, adopting the WKB approximation, we derive formulas for σ_F within the framework of the EFB model for a realistic nucleus-nucleus system considering absorption under the barrier. Section IV presents the numerical results. We summarize our findings in Sec. V.

II. RELATION BETWEEN DRM AND EFB MODELS

A. Absorption cross section through a complex rectangular potential with a well and a barrier

In order to understand the role of absorption in the nucleus-nucleus reaction qualitatively, let us consider the s-wave S matrix generated by the potential

$$U(r)=\begin{cases}-U_0-iW_0, & 0<r<a,\\ U_B-iW_B, & a<r<r_0,\\ U_B-iW_B', & r_0<r<b,\\ 0, & r>b.\end{cases} \tag{3}$$

The potential has a pocket in the region $r<a$, called $U_{\rm int}$, and a barrier in $a<r<b$, called $U_{\rm bar}$. $U_{\rm int}$ is accompanied by a strong imaginary potential W_0, whereas $U_{\rm bar}$ is made less absorptive. Further, the region of $U_{\rm bar}$ is divided into two zones having the inner zone $(a-r_0)$ more absorptive as compared to the outer zone (r_0-b). This simplified form of potential bears the characteristic features of a nucleus-nucleus potential which has a strong absorptive pocket inside and a barrier outside, having a complex nature with different strengths on either side of the barrier position R_B. Thus $W_0>W_B>W_B'$ and they may be conceptualized as a volume term, surface-peaked term, and direct reaction term, respectively, in accordance with the separation of whole range of the imaginary part of the OMP as suggested by Satchler [15].

We start with the modified radial equation for $U(r)$ for $l=0$:

$$\frac{d^2\phi(r)}{dr^2}+[k^2-V(r)]\phi(r)=0. \tag{4}$$

The radial solution is

$$\psi(r)=\frac{\phi(r)}{r}, \tag{5}$$

$$k^2=\frac{2\mu E}{\hbar^2}, \quad V(r)=\frac{2\mu}{\hbar^2}\,U(r). \tag{6}$$

Here μ indicates the mass of the particle and E stands for the incident center-of-mass energy. The solution of Eq. (4) can be written as

$$\phi_{\rm I}=\frac{1}{2i}\,[e^{i\alpha(r+a)}-e^{-i\alpha(r-a)}], \quad 0<r<a, \tag{7}$$

$$\phi_{\rm II}=\widetilde{A}e^{i\beta(r_0-r)}+\widetilde{B}e^{i\beta(r_0+r)}, \quad a<r<r_0, \tag{8}$$

$$\phi_{\rm III}=\widetilde{C}e^{i\beta'(b-r)}+\widetilde{D}e^{i\beta'(b+r)}, \quad r_0<r<b, \tag{9}$$

$$\phi_{\rm IV}=F_-e^{-ikr}+F_+e^{ikr}, \quad r>b, \tag{10}$$

where

$$\alpha^2=\frac{2\mu}{\hbar^2}\,(E+U_0+iW_0), \tag{11}$$

$$\beta^2=\frac{2\mu}{\hbar^2}\,(E-U_B+iW_B), \tag{12}$$

$$\beta'^2=\frac{2\mu}{\hbar^2}\,(E-U_B+iW_B') \tag{13}$$

and

$$\widetilde{A}=\frac{1}{2}\,e^{-i\beta(r_0-a)}\left[\frac{1}{2i}\,(e^{2i\alpha a}-1)-\frac{\alpha}{2i\beta}\,(e^{2i\alpha a}+1)\right], \tag{14}$$

$$\widetilde{B}=\frac{1}{2}\,e^{-i\beta(r_0+a)}\left[\frac{1}{2i}\,(e^{2i\alpha a}-1)+\frac{\alpha}{2i\beta}\,(e^{2i\alpha a}+1)\right], \tag{15}$$

$$\widetilde{C}=\frac{1}{2}\,e^{-i\beta'(b-r_0)}\left[\widetilde{A}\left(1+\frac{\beta}{\beta'}\right)+\widetilde{B}e^{2i\beta r_0}\left(1-\frac{\beta}{\beta'}\right)\right], \tag{16}$$

$$\widetilde{D}=\frac{1}{2}\,e^{-i\beta'(b+r_0)}\left[\widetilde{A}\left(1-\frac{\beta}{\beta'}\right)+\widetilde{B}e^{2i\beta r_0}\left(1+\frac{\beta}{\beta'}\right)\right], \tag{17}$$

$$F_-=\frac{1}{2}\,e^{ikb}\left[\widetilde{C}\left(1+\frac{\beta'}{k}\right)+\widetilde{D}e^{2i\beta' b}\left(1-\frac{\beta'}{k}\right)\right], \tag{18}$$

$$F_+=\frac{1}{2}\,e^{-ikb}\left[\widetilde{C}\left(1-\frac{\beta'}{k}\right)+\widetilde{D}e^{2i\beta' b}\left(1+\frac{\beta'}{k}\right)\right]. \tag{19}$$

The s-wave S matrix is given by

$$S=-\frac{F_+}{F_-}. \tag{20}$$

The expression for absorption cross section is written as

$$\sigma_{\rm rec}=\frac{\pi}{k^2}\,(1-|S|^2)\,. \tag{21}$$

Taking the complex conjugate of Eq. (4), we have

$$\frac{d^2\phi^*(r)}{dr^2}+[k^2-V^*(r)]\phi^*(r)=0. \tag{22}$$

Using Eqs. (4) and (22), we find

$$\phi^*\,\frac{d^2\phi}{dr^2}-\phi\,\frac{d^2\phi^*}{dr^2}=[2i\ \mathrm{Im}\ V(r)]\phi\phi^*, \tag{23}$$

where Im $V(r)$ stands for imaginary part of $V(r)$. Integrating this equation in the limit 0 to b, we get

$$\phi^*\,\frac{d\phi}{dr}-\phi\,\frac{d\phi^*}{dr}=\int_0^b[2i\ \mathrm{Im}\ V(r)]\phi\phi^*dr. \tag{24}$$

Now $\phi(r=0)=0$ and $\phi^*(r=0)=0$. So there is no contribution from the lower limit. Using the wave function $\phi(r)$ given by Eq. (10) at $r=b$ on the left-hand side of Eq. (24), we find

$$2ik(|F_+|^2-|F_-|^2)=\int_0^b[2i\ \mathrm{Im}\ V(r)]\phi\phi^*dr. \tag{25}$$

With the definition of the S matrix given by Eq. (20), Eq. (25) yields

$$1-|S|^2=I_1+I_2+I_3, \tag{26}$$

where

$$I_1=-\frac{1}{k}\int_0^a \mathrm{Im}\ V(r)\left|\frac{\phi}{F_-}\right|^2dr, \tag{27}$$

$$I_2=-\frac{1}{k}\int_a^{r_0} \mathrm{Im}\ V(r)\left|\frac{\phi}{F_-}\right|^2dr, \tag{28}$$

$$I_3=-\frac{1}{k}\int_{r_0}^b \mathrm{Im}\ V(r)\left|\frac{\phi}{F_-}\right|^2dr. \tag{29}$$

Now using the potentials given by the expression (3) and corresponding wave functions given by Eqs. (7)–(9), in different regions, we simplify the integrals in Eqs. (27), (28), and (29) and obtain

$$I_1=\frac{2\mu}{\hbar^2}\,\frac{W_0}{4k|F_-|^2}\left[\frac{1-e^{-4a\alpha_i}}{2\alpha_i}-\frac{e^{-2a\alpha_i}}{\alpha_r}\sin(2a\alpha_r)\right], \tag{30}$$

where $\alpha_i=\mathrm{Im}\ \alpha$ and $\alpha_r=\mathrm{Re}\ \alpha$ with the symbols Re and Im indicating real and imaginary parts, respectively. Here F_- is given by Eq. (18):

$$I_2=\frac{2\mu}{\hbar^2}\frac{W_B}{k|F_-|^2}e^{-2\beta_i r_0}\left[\frac{1}{2\beta_i}|\widetilde{A}|^2(e^{2\beta_i r_0}-e^{2\beta_i a})\right.$$
$$-\frac{1}{2\beta_i}|\widetilde{B}|^2(e^{-2\beta_i r_0}-e^{-2\beta_i a})$$
$$\left.+\frac{1}{\beta_r}\,\mathrm{Im}\{\widetilde{A}^*\widetilde{B}(e^{2i\beta_r r_0}-e^{2i\beta_r a})\}\right], \tag{31}$$

where $\beta_i=\mathrm{Im}\,\beta$ and $\beta_r=\mathrm{Re}\,\beta$,

$$I_3=\frac{2\mu}{\hbar^2}\frac{W'_B}{k|F_-|^2}e^{-2\beta'_i b}\left[\frac{1}{2\beta'_i}|\widetilde{C}|^2(e^{2\beta'_i b}-e^{2\beta'_i r_0})\right.$$
$$-\frac{1}{2\beta'_i}|\widetilde{D}|^2(e^{-2\beta'_i b}-e^{-2\beta'_i r_0})$$
$$\left.+\frac{1}{\beta'_r}\,\mathrm{Im}\{\widetilde{C}^*\widetilde{D}(e^{2i\beta'_r b}-e^{2i\beta'_r r_0})\}\right], \tag{32}$$

where $\beta'_i=\mathrm{Im}\,\beta$ and $\beta'_r=\mathrm{Re}\,\beta$. By using the expressions (30)–(32) in Eq. (26) and subsequently through Eq. (21), one can estimate the absorption cross section from different regions of the potential. Thus, in the region $0-r_0$, we obtain the absorption cross section as

$$\sigma_{\mathrm{rec}}=\frac{\pi}{k^2}(I_1+I_2). \tag{33}$$

This corresponds to the fusion cross section in the DRM of fusion [8].

B. Fusion cross section from transmission across complex barrier

We now estimate the cross section within the framework of one-dimensional transmission across a potential barrier based on which the EFB model is developed. Let us consider the barrier to be complex with strength $U_B-iW'_B$ and situated in the region $r_0<r<b$ with a width $d=b-r_0$. The transmission coefficient (T_C) across this barrier is given by

$$T_C=|H|^2, \tag{34}$$

where

$$H=\frac{4\gamma k e^{-ikd}}{(\gamma+k)^2e^{-i\gamma d}-(\gamma-k)^2e^{i\gamma d}}, \tag{35}$$

with $\gamma^2=(2\mu/\hbar^2)(E-U_B+iW'_B)$ and k is expressed as in Eq. (6). Then the corresponding cross section is expressed as

$$\sigma'_F=\frac{\pi}{k^2}T_C. \tag{36}$$

Thus σ'_F represents the fusion cross section with regard to the EFB model.

The success of the DRM and EFB model indicates that for a suitable value of r_0 the cross sections σ_{rec} given by Eq. (33) and σ'_F given by Eq. (36) can be expected to give similar results. In the language of the DRM and EFB model, r_0 corresponds to the fusion radius parameter R_F.

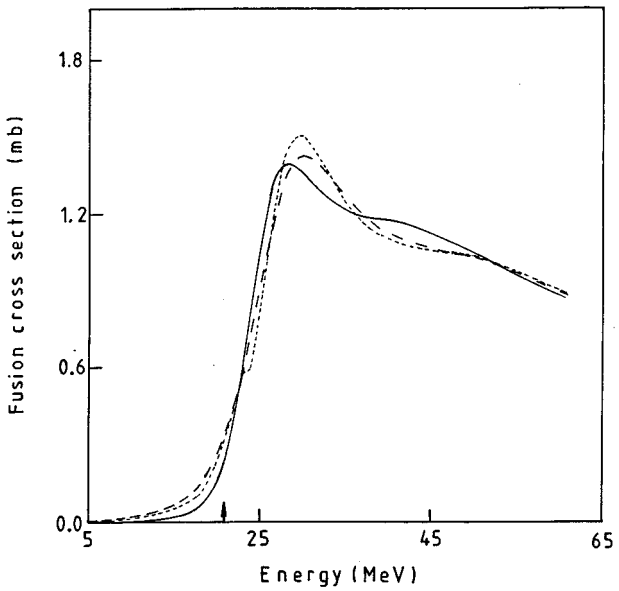

FIG. 1. Comparison of various fusion cross sections σ_{rec} [Eq. (33)], σ'_F [Eq. (36)], and σ_F [Eq. (38)] represented by solid, long dashed, and short dashed curves, respectively. The potential parameters used are $U_0=50$ MeV, $W_0=20$ MeV, $U_B=21.01$ MeV, $W_B=10$ MeV, $W'_B=1$ MeV, $a=7$ fm, $b=11$ fm, and $r_0=9.5$ fm. The arrow indicates U_B.

We further look into the development of expression (36) on the perspective of the survival probability of the incident flux against absorption during crossing of the complex barrier in the region r_0-b. The probability factor P_S, introduced by Eq. (2), accounting for the absorption under the barrier can be simplified to give

$$P_S=e^{-2W'_B\tau/\hbar}, \tag{37}$$

where $\tau(=d/[2(E-U_B)/\mu]^{1/2})$ is the transit time of the barrier of width $d=b-r_0$ in the real trajectory. The transmitted flux through the complex barrier can be represented by the product T_RP_S, where T_R is the transmission coefficient of the corresponding real barrier and the corresponding fusion cross section is given by

$$\sigma_F=\frac{\pi}{k^2}T_RP_S. \tag{38}$$

It is of interest to compare the results of σ_{rec}, σ'_F, and σ_F given by Eqs. (33), (36), and (38), respectively, at different energies. In Fig. 1, we do so by applying the formulation to a specific square well potential specified by $U_0=50$ MeV, $W_0=20$ MeV, $W_B=10$ MeV, $W'_B=1$ MeV, $a=7$ fm, $b=11$ fm, and $r_0=9.5$ fm. The height of the barrier is $U_B=21.01$ MeV. This value of the barrier height approximately corresponds to the nucleus-nucleus system $^{16}\mathrm{O}+^{28}\mathrm{Si}$, and we have used these mass numbers to calculate k^2, α^2, β^2, $(\beta')^2$, etc. in our calculations. These calculations were done for s waves in the energy range from $E=1$ to 60 MeV. It is

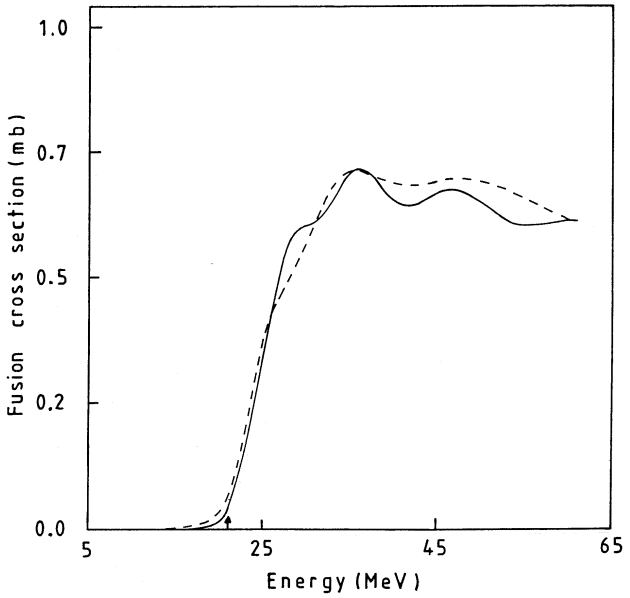

FIG. 2. Comparison of fusion cross sections for DRM ($\sigma_{\rm rec}$) and EFB (σ_F') concepts shown by solid and dashed curves, respectively, for a rectangular potential

$$U(r)=\begin{cases}-U_0-iW_0, & \text{if } r<a,\\ U_B-iW_B, & \text{if } a<r<b,\\ 0, & \text{if } r>b,\end{cases}$$

where $U_0=50$ MeV, $W_0=20$ MeV, $U_B=21.01$ MeV, $W_B=2$ MeV, $a=6$ fm, $b=9.5$ fm, and the EFB width $d=2.5$ fm. The arrow indicates U_B.

seen that all three results of the cross sections are very close to each other. This important finding leads us to the following conclusions.

(i) The similarity of $\sigma_{\rm rec}$ and σ_F' proves that the DRM and EFB concepts of fusion are complementary to each other.

(ii) The equivalence of σ_F' and σ_F justifies the splitting of transmitted flux through a complex barrier into transmission through a real barrier and a survival probability factor depending upon the imaginary potential within the barrier and the time of transit across this region.

The similarity of $\sigma_{\rm rec}$ and σ_F' was verified even in the case of a rectangular barrier with constant absorption W_B in the entire region $a<r<b$. In Fig. 2, we show a typical result where σ_F' and $\sigma_{\rm rec}$ are compared. This further strengthens the conclusion (i) stated above.

The problem of estimating the fusion cross section in the case of a nucleus-nucleus reaction with its optical potential in Woods-Saxon form becomes easier by the use of formula (38) as compared to Eq. (36), which uses an exact transmission coefficient across this complex barrier. This is because one can avoid the complex turning point WKB approach since one uses a real barrier in obtaining Eq. (38). Further, by adopting this procedure, one can avoid the complexity of calculating the absorption cross section generated within the interior region where the nucleus-nucleus potential is not fully explored. In the next section, we adopt a general procedure of developing the formula (38) to calculate the fusion cross section for HI collisions using a more realistic nucleus-nucleus potential and including all relevant partial waves.

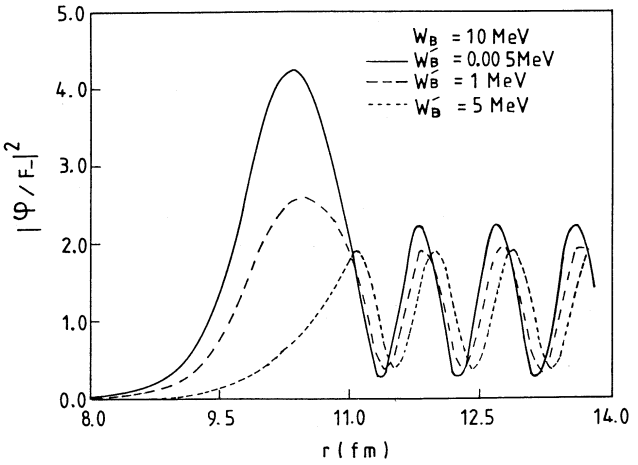

FIG. 3. Variation of $|\phi/F_-|^2$ as a function of radial separation r. Curves corresponding to different values of W_B' but with fixed $W_B=10$ MeV are labeled in the inset. The potential parameters used are $U_0=50$ MeV, $W_0=20$ MeV, $U_B=21.01$ MeV, $a=7$ fm, $b=11$ fm, and $r_0=9.5$ fm.

Before we conclude this section, we wish to analyze the effect of the imaginary potentials W_B' and W_B on the amplitude of the wave function represented by the term $|\phi/F_-|^2$ in the interior region ($r<r_0$). It is found that $|\phi/F_-|^2$ substantially decreases with the small increase of W_B' (see Fig. 3) for a given value of W_B. Thus a small imaginary potential in the outer zone of the barrier controls the flux going into the inner zone of the barrier as a controlling gate. This is consistent with the role of the factor $P_S=e^{-2W_B'\tau/\hbar}$ used in the formula (38). Further, we see in Fig. 4 that $|\phi/F_-|^2$ becomes very small within a short distance from r_0 inward in the presence of a larger imaginary potential W_B in this interior region. As a result of this, the reaction cross section from the region 0 $-r_0$ is mostly equal to that obtained from the region $a-r_0$ under the barrier. This result strongly supports the conjecture that the whole of the fusion process in the HI reaction is possibly completed under the barrier, i.e., within the region

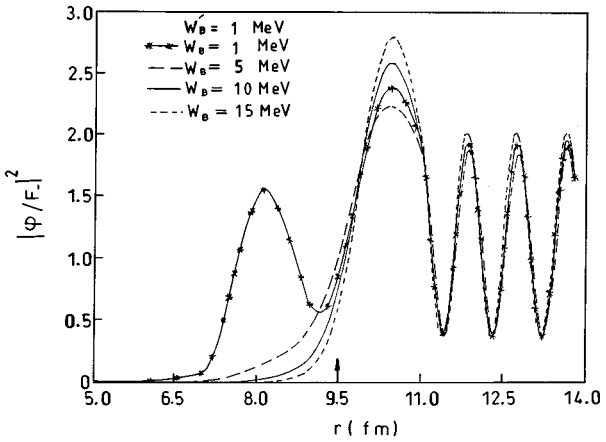

FIG. 4. Same as Fig. 3. Curves corresponding to different values of W_B but with fixed $W_B'=1$ MeV are labeled in the inset. Other potential parameters are the same as those in Fig. 3. The arrow indicates the point $r_0=9.5$ fm.

inside but close to the position of the peak of effective barrier.

III. FORMULATION FOR THE NUCLEUS-NUCLEUS FUSION CROSS SECTION

Having established the fact that the total absorption within a region from the origin to a point $r=r_0=R_F$ close to the Coulomb barrier radius (R_B) as in the DRM of fusion is equivalent to the cross section obtained from the transmission across the remainder of the complex barrier from outside to that particular point R_F as in the EFB model, it would now suffice to calculate the transmission coefficient of the following complex effective barrier:

$$U(l,r)=\begin{cases} U_N(r)+U_C(r)+U_l(r), & r\geqslant R_F, \\ 0, & r<R_F, \end{cases} \tag{39}$$

where $U_l=(\hbar^2/2\mu)[l(l+1)/r^2]$, with μ denoting the reduced mass, $U_C(r)$ is the usual form of the nucleus-nucleus electrostatic potential with radius parameter r_C, and the nuclear part $U_N(r)$ is expressed as

$$U_N(r)=-Ug(R_U,a_U,r)-iWg(R_W,a_W,r),$$

where the commonly used expression for $g(R_j,a_j,r)$ is the Woods-Saxon form factor given by

$$g(R_j,a_j,r)=\left[1+\exp\left(\frac{r-R_j}{a_j}\right)\right]^{-1},$$

where $R_j=r_j(A_1^{1/3}+A_2^{1/3})$ with $j=1,2$ and $R_1=R_U$, $r_1=r_U$, $a_1=a_U$, $R_2=R_W$, $r_2=r_W$, and $a_2=a_W$. The quantities r_j and a_j are the radius and diffuseness parameters in fm, and U and W are the depths in MeV for the real and imaginary parts of the OMP, respectively. A_1 and A_2 are the mass numbers of the two colliding nuclei having corresponding proton numbers denoted by Z_1 and Z_2. In the earlier formulation of the EFB, W in the barrier region was assumed to be negligible (zero).

On the basis of the results discussed in the last section, the transmission coefficient of the above complex potential can be equated to the product of the transmission coefficient (T_{Rl}) in the real trajectory and a survival probability factor P_{Sl} equivalent to Eq. (37) in the lth partial wave. Then the total fusion cross section is estimated by the expression

$$\sigma_F=\frac{\pi}{k^2}\sum_{l=0}^{\infty}(2l+1)T_{Rl}P_{Sl}. \tag{40}$$

The contribution from each l or the spin distribution (σ_F^l) at a certain $E_{\text{c.m.}}$ is represented by

$$\sigma_F^l=\frac{\pi}{k^2}(2l+1)T_{Rl}P_{Sl}. \tag{41}$$

At the same energy, the average angular momenta of the fused body, denoted by $\langle l\rangle$, is expressed as

$$\langle l\rangle=\frac{\Sigma_{l=0}^{\infty}l\sigma_F^l}{\sigma_F}. \tag{42}$$

We now obtain the complete expressions for T_{Rl} and P_{Sl}.

A. General expression for T_{Rl} along a real trajectory

The real part of the potential given by Eq. (39) is a smoothly varying potential with a peak at $r=R_F=a$ (say) and decreases with an increase of r. We visualize this potential as slowly varying within the region $a\leqslant r<b$ and zero in the outer region $r>b$, where $b\gg a$. Thus the first-order WKB approximation for the wave function is suitable and it guarantees the conservation of particles [12]. However, when the points a and b are very close to each other, the WKB approximation for the wave function would substantially deviate from the exact wave function [16]. In this critical situation, one can use the zeroth-order WKB approximation, which readily conserves the particles [12]. Following the mathematical procedure given by Farina [12] (also see Ref. [11]), we obtain the transmission coefficient through such a real potential barrier and the results are summarized below.

Let U_{EB}^l denote the height of the effective barrier given by Eq. (39) in the lth partial wave at the radial position $r=a=R_F$. For $E_{\text{c.m.}}<U_{\text{EB}}^l$, the transmission coefficient below the barrier ($T_{Rl}^{(bb)}$) is given by

$$T_{Rl}^{(bb)}=\frac{4\hat{P}_a\hat{P}_b}{(\hat{P}_a+\hat{P}_b)^2+[k^2+(\hat{P}_a\hat{P}_b/k)^2+\hat{P}_a^2+\hat{P}_b^2]\sinh^2\hat{P}_{ab}} \tag{43}$$

where $\hat{P}_a=\sqrt{V(l,r=a)-k^2}$, $\hat{P}_b=\sqrt{V(l,r=b)-k^2}$, and

$$\hat{P}_{ab}=\int_a^b\sqrt{V(l,r)-k^2}\,dr, \tag{44}$$

with $V(l,r)=(2\mu/\hbar^2)U(l,r)$.

Discontinuities in the potential at $r=a$ and $r=b$ introduce nonclassical phenomena, and so, in the below-barrier situation, we may assume $|\hat{P}_a|=|\hat{P}_b|=k$ [12]. With this, Eq. (43) reduces to

$$T_{Rl}^{(bb)}=\frac{1}{\cosh^2\hat{P}_{ab}}, \quad E_{\text{c.m.}}<U_{\text{EB}}^l. \tag{45}$$

The integral for $\hat{P}_{ab}$ given in Eq. (44) is evaluated numerically for positive values of $V(l,r)-k^2$. However, for $E_{\text{c.m.}}\approx U_{\text{EB}}^l$, the point $r=b$ approaches the point $r=a$ so that $\hat{P}_b\approx\hat{P}_a$, and in this situation one can express $\hat{P}_{ab}$ approximately as $\hat{P}_{ab}\approx\hat{P}_a d$, where $d=b-a$ is a very small distance. With this approximation, Eq. (43) can be written as

$$T_{Rl}^{(bb)}=\left[1+\frac{(k^2+\hat{P}_a^2)^2}{4k^2\hat{P}_a^2}\sinh^2(\hat{P}_a d)\right]^{-1}, \quad E_{\text{c.m.}}\approx U_{\text{EB}}^l. \tag{46}$$

It may be pointed out that in this situation we find $\hat{P}_a\ll k$, $\hat{P}_a d\ll 1$ and the above expression is very sensitive to the value of d. Having set $d=\pi/2k$, Eq. (46) gives a value $T_{Rl}^{(bb)}\approx 0.61$, which is found to be very close to the exact numerical result for energy near the barrier of a model potential (see Table I of Ref. [9]) Thus $d=\pi/2k$, which is equal to a quarter of the de Broglie wavelength, is a critical

distance over which we do not expect much change in the total effective potential $U(l,r)$ suited for the WKB approximation. One observes such a situation in the case of a few l's in the neighborhood of the grazing partial wave l_g defined by the condition $E_{\rm c.m.}=U^{l_g}_{\rm EB}$. The values of $T^{(bb)}_{Rl}$ given by Eqs. (45) and (46) in their respective limiting situations can be accounted for by the unified expression

$$T^{(bb)}_{Rl}=\frac{0.61}{\cosh^2\,\hat{P}_{ab}},\quad E_{\rm c.m.}\leqslant U^{l}_{\rm EB}. \tag{47}$$

Coming to the above barrier situation ($E_{\rm c.m.}>U^{l}_{\rm EB}$), the transmission coefficient ($T^{(ab)}_{Rl}$) is expressed as

$$T^{(ab)}_{Rl}=\frac{4P_aP_b}{(P_a+P_b)^2+[k^2+(P_aP_b/k)^2-P_a^2-P_b^2]\sin^2\,P_{ab}}, \tag{48}$$

where $P_a=\sqrt{k^2-V(l,r=a)}$, $P_b=\sqrt{k^2-V(l,r=b)}$, and

$$P_{ab}=\int_a^b\sqrt{k^2-V(l,r)}\;dr. \tag{49}$$

Here, also, we visualize a similar situation for $E_{\rm c.m.}\approx U^{l}_{\rm EB}$, where the point $r=b$ is expected to be close to $r=a$. Hence we have $P_b\approx P_a=\sqrt{k^2-V(l,r=a)}$ and P_{ab} given by Eq. (49) reduces to $P_{ab}=P_ad$, where $d=(b-a)=\pi/2k$. However, for $E_{\rm c.m.}>U^{l}_{\rm EB}$, we may set $P_b\approx k$ considering $b>a$ such that $V(l,r=b)$ is negligibly small. With these assumptions, Eq. (48) reduces to

$$T^{(ab)}_{Rl}=\left[1+\frac{(k^2-P_a^2)^2}{4k^2P_a^2}\sin^2\,P_ad\right]^{-1},\quad E_{\rm c.m.}\approx U^{l}_{\rm EB}, \tag{50}$$

$$T^{(ab)}_{Rl}=\frac{4kP_a}{(k+P_a)^2},\quad E_{\rm c.m.}>U^{l}_{\rm EB}. \tag{51}$$

Clearly Eq. (50) gives $T^{(ab)}_{Rl}=0.61$ for a few partial waves in the situation $E_{\rm c.m.}\approx U^{l}_{\rm EB}$, where $P_a\ll k$ and $P_ad\ll 1$, with $d=\pi/2$k. Thus Eqs. (47) and (50) give similar results near the barrier, though the former approaches the top of the barrier from below and the latter from above.

Thus, for the estimate of σ_F through Eq. (40), the results of transmission coefficients T_{Rl} are obtained by using the expression (47) for the below-barrier case and expressions (50) and (51) for above-barrier energies.

B. Expression for the survival probability factor P_{Sl}

The probability factor for survival from absorption represented by Eq. (2) can be expressed for different l's in the barrier region as

$$P_{Sl}=\exp\left[-\int_{R_F}^{\infty}\frac{\overline{W}(r)}{\kappa_l(r)}\,dr\right], \tag{52}$$

where $\kappa_l^2(r)=|k^2-V(l,r)|$. Here $\overline{W}(r)=\overline{W}g(R_W,a_W,r)$ with $\overline{W}=(2\mu/\hbar^2)W$ indicating the imaginary part of the OMP presented in Eq. (39). For a given l, we obtain the results of P_{Sl} by numerical integration in the real trajectory. However, close examination of expression (52) reveals that at $E_{\rm c.m.}\approx U^{l}_{\rm EB}$ the transit time becomes very large, which results in $P_{Sl}\ll 1$ for a few l's near l_g. In this critical situation of classical orbiting, which is equivalent to quantal resonance states, the width of absorption [17] can be expressed as

$$\Gamma=\hbar\omega_{Bl}+2W_{\rm av}, \tag{53}$$

where ω_{Bl} is the frequency with respect to a parabolic approximation to the effective potential barrier having its peak at $r=R_{Bl}$ in the lth partial wave. $W_{\rm av}$ denotes the average imaginary potential near the barrier, and it is approximately taken as $W_{\rm av}=W(r=R_F)\approx W\,\exp[(R_W-R_F)/a_W]$. Then the survival probability in this situation is given by

$$P_{Sl}=\exp\left[\frac{-2W_{\rm av}}{\hbar\omega_{Bl}+2W_{\rm av}}\right]. \tag{54}$$

In the cases of heavy ion systems, we have found that $\hbar\omega_{Bl}\approx 4$ MeV (see, for example, Table II, and, also, Ref. [17]) and does not vary much with different l's. As a result, $P_{Sl}\approx 1$ because $W_{\rm av}<1$ MeV for a given $R_F\geqslant R_B$.

Using the expression (52) with the necessary correction (54) and the expressions (47), (50), and (51) for T_{Rl} derived earlier, we estimate total σ_F by Eq. (40) and the corresponding average angular momenta $\langle l\rangle$ by Eq. (42) at different $E_{\rm c.m.}$ in the cases of realistic nucleus-nucleus systems. Let us denote these results by $\sigma_F^{(\rm MWKB)}$ and $\langle l\rangle^{(\rm MWKB)}$, respectively, as their derivation is based on the modified WKB approximation.

IV. NUMERICAL RESULTS AND DISCUSSION

In this section, we apply the formulation presented in the previous section to the simultaneous analysis of the experimental results of σ_F and $\langle l\rangle$ as a function of $E_{\rm c.m.}$ near the Coulomb barrier energy in the cases of several HI systems. We also compare our results $\sigma_F^{(\rm MWKB)}$ and $\langle l\rangle^{(\rm MWKB)}$ with those obtained using DRM [8] and CC calculations. Let us denote the results of σ_F and $\langle l\rangle$ of the CC calculation by $\sigma_F^{(\rm CC)}$ and $\langle l\rangle^{(\rm CC)}$, those of the DRM by $\sigma_F^{(\rm DRM)}$ and $\langle l\rangle^{(\rm DRM)}$, and from experiment by $\sigma_F^{(\rm expt)}$ and $\langle l\rangle^{(\rm expt)}$.

The results of $\sigma_F^{(\rm MWKB)}$ along with $\langle l\rangle^{(\rm MWKB)}$ in Figs. 5, 6, and 8–11 and $\sigma_F^{(\rm MWKB)}$ alone in Fig. 7 are shown by solid curves. They are compared with the corresponding $\sigma_F^{(\rm expt)}$ and $\langle l\rangle^{(\rm expt)}$ data at different $E_{\rm c.m.}$ for the systems ^{16}O+^{152}Sm (Fig. 5), ^{16}O+^{154}Sm (Fig. 6), ^{58}Ni+^{58,64}Ni (Fig. 7), ^{58}Ni+^{64}Ni (Fig. 8), ^{64}Ni+^{64}Ni (Fig. 9), ^{64}Ni+^{92}Zr (Fig. 10), and ^{64}Ni+^{100}Mo (Fig. 11). It is seen that in all cases the respective data are explained quite satisfactorily over the whole range of energy studied. References [8,18–21], from which these data were taken, are all listed in Table I. In this table, we also list the OMP parameters used in our calculation for different systems along with their respective references. As the ^{64}Ni+^{92}Zr system is a nearest neighbor of ^{64}Ni+^{100}Mo, we have used the OMP of the latter system in the study of the former pair. In this case (Fig. 10), given the proper OMP parameters, we expect a better fit to the respective experimental data by $\sigma_F^{(\rm MWKB)}$ and $\langle l\rangle^{(\rm MWKB)}$. In Table

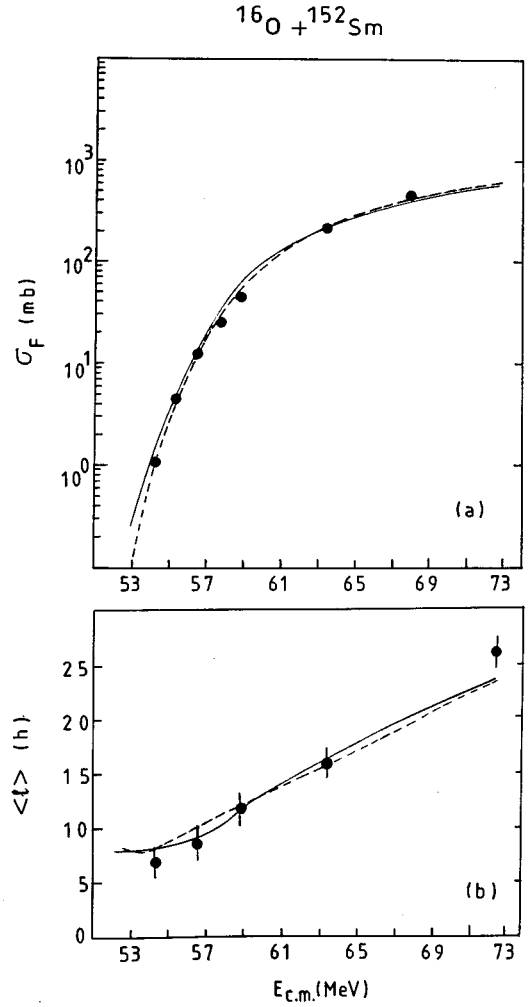

FIG. 5. Variation of (a) fusion cross section σ_F and (b) average angular momenta $\langle l \rangle$ as a function of $E_{\text{c.m.}}$ for the $^{16}\text{O}+^{152}\text{Sm}$ system. The solid curves represent the values of σ_F^{MWKB} and $\langle l \rangle^{\text{MWKB}}$. The corresponding values from experiment (solid points) and CC calculations (dashed curves) have been taken from Ref. [19].

II, we give the values of the s-wave barrier height U_B, its position R_B, and curvature factor $\hbar\omega_B$ obtained by using the corresponding OMP for different systems. The values of R_F along with the radius parameter $r_F = R_F/(A_1^{1/3}+A_2^{1/3})$ in brackets are also listed in this table. We observe that in all the cases $r_F \sim 1.4$ fm and in most of the cases $R_F > R_B$. In the cases of asymmetric pairs, R_F is very close to R_B. This result implies that the process of fusion is initiated before the participants reach the barrier position and it is seen to be earlier in the cases of nearly or very symmetric systems as compared to asymmetric pairs.

In Fig. 7, we show the results $\sigma_F^{(\text{DRM})}$ by dashed curves. On comparison with $\sigma_F^{(\text{MWKB})}$ (solid curves) in this figure, we find that our results are very close to those of the DRM in the case of $^{58}\text{Ni}+^{58}\text{Ni}$ and both explain the data well. In the case of $^{58}\text{Ni}+^{64}\text{Ni}$, of course, $\sigma_F^{(\text{MWKB})}$ is found to be closer to $\sigma_F^{(\text{expt})}$. Using the formulation of the DRM, the $\sigma_F^{(\text{expt})}$ for the reaction $^{64}\text{Ni}+^{100}\text{Mo}$ are analyzed in Ref. [21] with reasonable success. However, in this calculation, the radius pa-

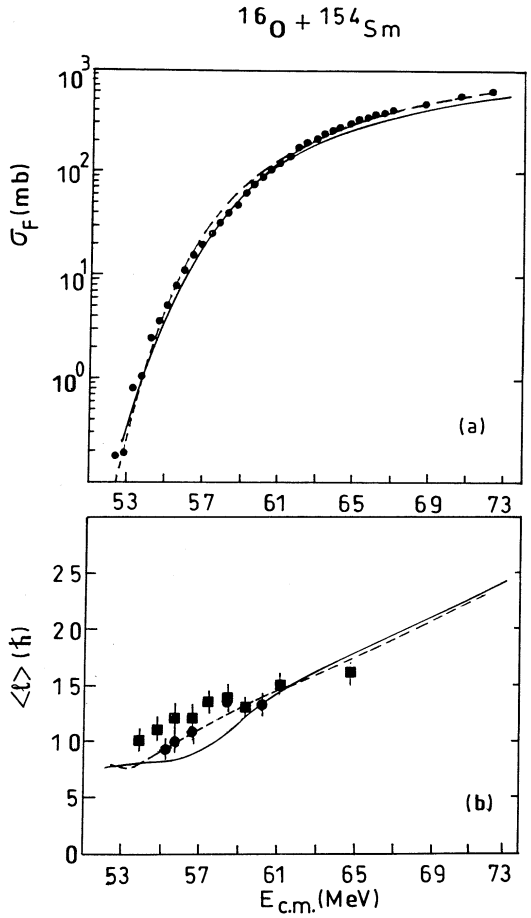

FIG. 6. Same as Fig. 5 for $^{16}\text{O}+^{154}\text{Sm}$.

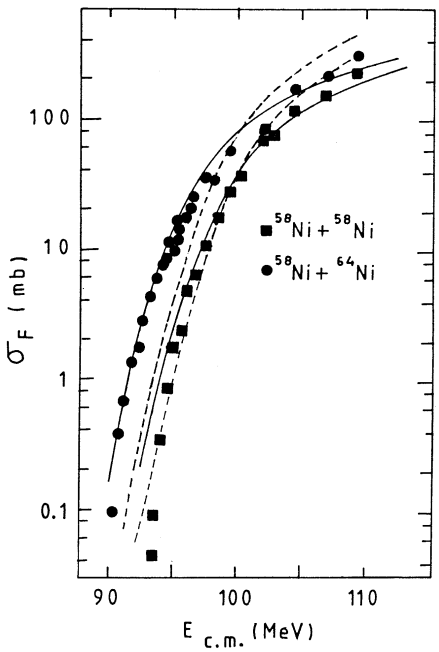

FIG. 7. Same as Fig. 5(a) for $^{58}\text{Ni}+^{58}\text{Ni}$ and $^{58}\text{Ni}+^{64}\text{Ni}$. Solid curves represent σ_F^{MWKB}. Here σ_F^{expt} (solid dots or squares) and σ_F^{DRM} (dashed curves) have been taken from Ref. [8].

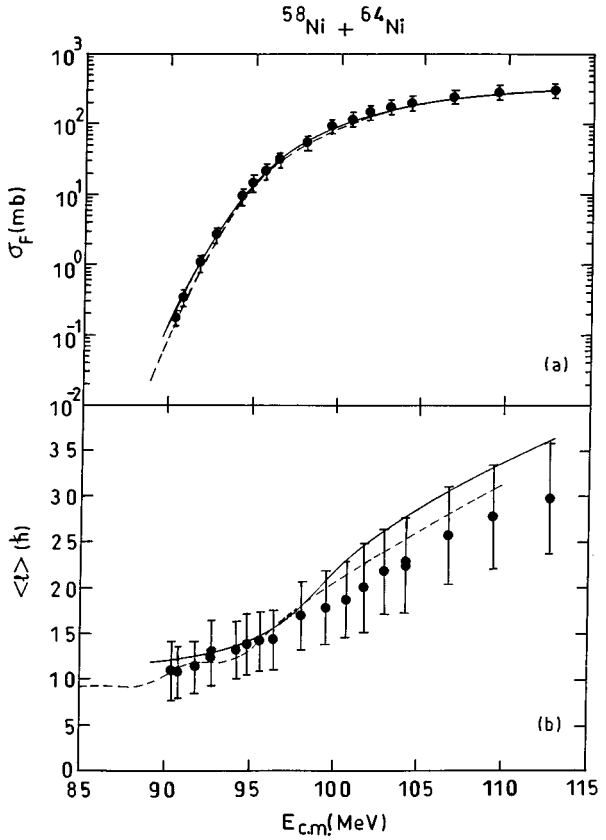

FIG. 8. Same as Fig. 5 for ^{58}Ni+^{64}Ni. Corresponding values of experimental data and CC calculations are obtained from Ref. [20].

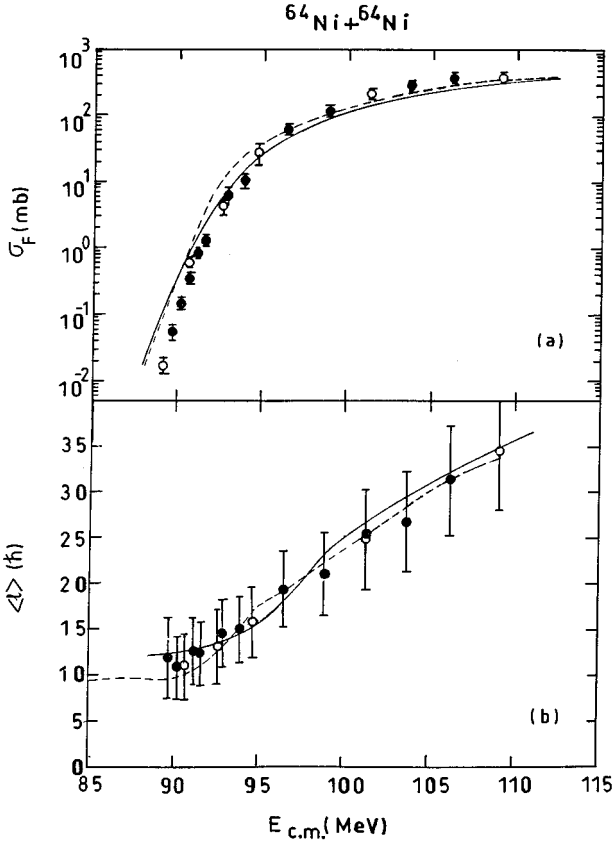

FIG. 9. Same as Fig. 5 for ^{64}Ni+^{64}Ni. Corresponding values of experimental data and CC calculations are obtained from Ref. [20].

rameter r_F was varied to fit the data, whereas in our calculation we have considered a fixed $r_F = 1.41$ fm for the whole energy range and obtained the results represented by solid curves in Fig. 11. The overall fit is seen to be quite good. However, the larger value of $\langle l \rangle^{(\mathrm{MWKB})}$ in the higher energy region, seen in Fig. 11(b), can be made close to $\langle l \rangle^{(\mathrm{expt})}$ if r_F is slightly decreased, as done in Ref. [21]. These comparative studies in the case of realistic nucleus-nucleus systems justify the conjecture that the EFB and DRM approaches are complementary to each other. In other words, they are two procedures describing the same physical phenomenon in different languages. Further, the results of $\sigma_F^{(\mathrm{CC})}$ and $\langle l \rangle^{(\mathrm{CC})}$ are obtained from the respective references for experimental data listed in Table I and are shown by dashed curves in the corresponding Figs. 5, 6, and 8–11. They successfully explain the corresponding experimental data of asymmetric (Figs. 5 and 6) and symmetric (Figs. 8 and 9) systems, but fail to do so in the cases of nearly symmetric pairs (Figs. 10 and 11). As already discussed, in all these cases, σ_F^{MWKB} and $\langle l \rangle^{\mathrm{MWKB}}$, represented by solid curves in these figures, provide a good fit to the corresponding measured data. This consistent result of the present formulation is remarkable in view of the failure of CC calculations in some cases.

In order to analyze the effect of the factor P_{Sl} in the fusion process, we have compared the results of σ_F^{MWKB}, which fit the data well with certain R_F in a given system, with the values of σ_F by setting $P_{Sl} = 1$ in the expression (40). We find that P_{Sl} has the tendency of reducing the values of σ_F with $P_{Sl} = 1$ by about 15%. This effect of the reduction of σ_F by P_{Sl} can be accounted for if one slightly decreases the value of R_F, having set $P_{Sl} = 1$, and can explain the data well. Hence one may ignore the use of imaginary part of the OMP in the outer region by choosing a suitable R_F for the estimate of σ_F within the framework of a one-dimensional transmission model. This assumption has been adopted in our earlier papers [9–11].

It may be pointed out, further, that the factor P_{Sl} given by Eq. (52) at a certain energy does not vary much with different l's except near l_g where it gives lower values. This can be corrected by the use of expression (54). However, for a given $E_{\mathrm{c.m.}}$, P_{Sl} approaches unity for larger l in the region $l > l_g$. This result may imply that higher l's under a subbarrier situation survive more against absorption. It should not be inferred that these l's contribute more to fusion, because, at the same time, the corresponding value of T_{Rl} decreases very fast with the increase of l in this region and, as a result, the product $T_{Rl}P_{Sl}$ yields very small values to give a decreasing value of σ_F^l with the increase of l beyond l_g. On the whole, the variation of σ_F^l with l at a certain energy is found to be consistent with the corresponding experimental spin distribution as demonstrated in Ref. [11]. The results of calculations for various other systems will be reported in a future publication.

V. SUMMARY AND CONCLUSION

The study of the HI reaction within the framework of the optical model potential theory envisages an imaginary part

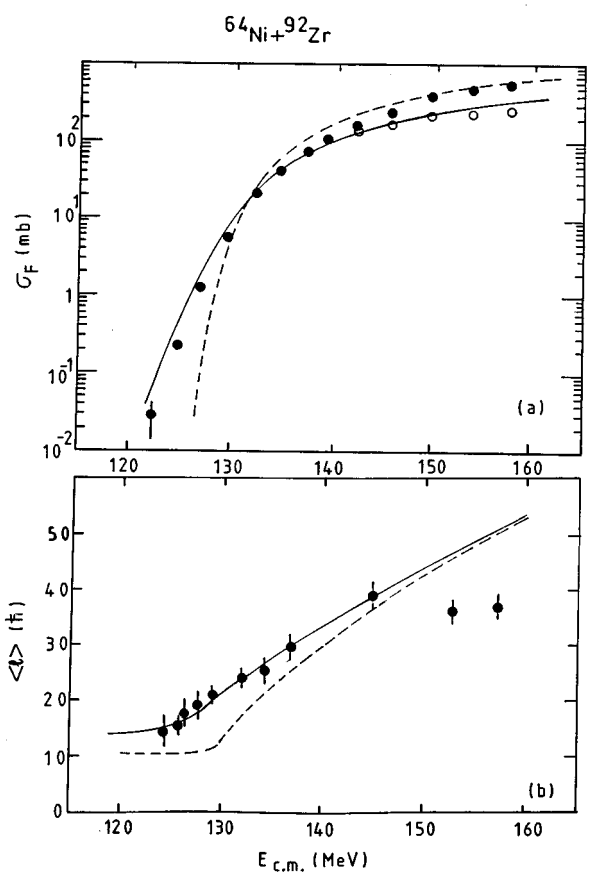

FIG. 10. Same as Fig. 5 for ^{64}Ni+^{92}Zr. Corresponding results from measurements and CC calculations are obtained from Ref. [18].

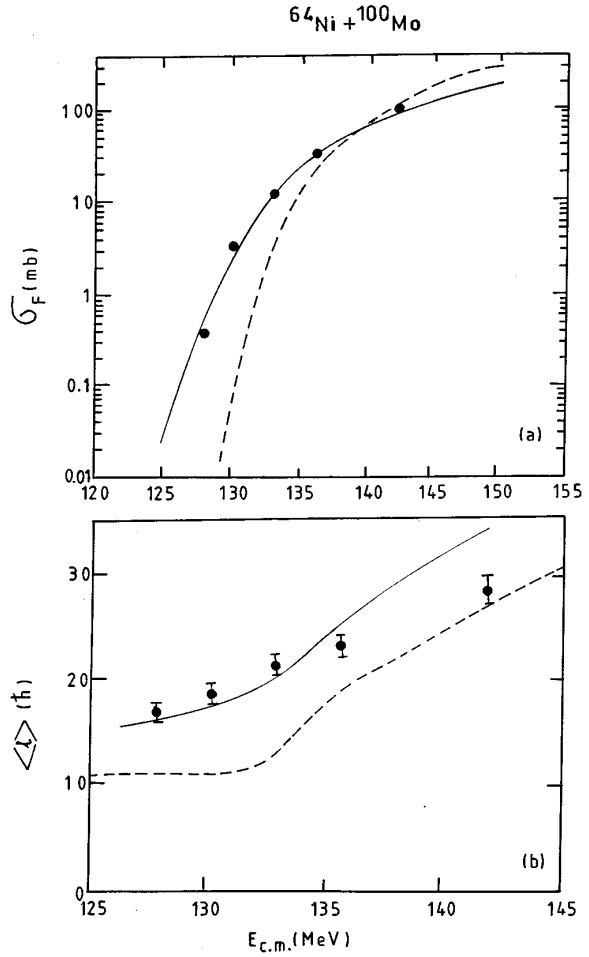

FIG. 11. Same as Fig. 5 for ^{64}Ni+^{100}Mo. Corresponding results from measurements and CC calculations are obtained from Refs. [18,21].

under a real potential showing a pocket inside followed by a barrier outside. This imaginary part of the potential governs the process of absorption to different channels including direct reactions not proceeding through the elastic channel. Incorporating this picture, the cross section σ_F for compound nucleus formation can be estimated from two different but complementary ways: (i) from the absorption in the interior region $(0-R_F)$ as in the DRM [8] and (ii) from the probability of reaching the same point R_F from outside as in the EFB transmission model [9–11]. In our previous calculations [9–11], we have assumed the barrier in the region $r>R_F$ to be real, and thereby the role of imaginary part of the potential addressing the peripheral processes has been neglected.

In the present calculation, the EFB transmission model is formulated utilizing the complex potential barrier to make it more sound and complete. For the estimate of σ_F, the transmission coefficient T_C across the complex barrier is equated to the product $T_{Rl}P_{Sl}$ where T_{Rl} indicates the transmission coefficient along a real trajectory specified by the partial wave l and P_{Sl} stands for the survival probability against absorption to peripheral processes in that trajectory. Before applying this formulation to realistic nucleus-nucleus reactions, we test the complementary nature of the DRM and

TABLE I. OMP parameters with their references for various HI systems. Also listed are the respective references for experimental σ_F and $\langle l \rangle$ data.

System	U (MeV)	W (MeV)	r_U (fm)	a_U (fm)	r_W (fm)	a_W (fm)	r_C (fm)	Reference OMP	Reference data
^{16}O+^{152}Sm	22.5	13	1.34	0.57	1.34	0.36	1.25	[19]	[19]
^{16}O+^{154}Sm	22.5	13	1.34	0.57	1.34	0.36	1.25	[19]	[19]
^{58}Ni+^{58}Ni	40	15	1.2	0.55	1.2	0.55	1.2	[8]	[8]
^{58}Ni+^{64}Ni	40	15	1.2	0.55	1.2	0.55	1.2	[8]	[8,20]
^{64}Ni+^{64}Ni	40	15	1.2	0.55	1.2	0.55	1.2	[8]	[20]
^{64}Ni+^{92}Zr	178	80	1.08727	0.707	1.08727	0.707	1.08727	[21]	[18]
^{64}Ni+^{100}Mo	178	80	1.08727	0.707	1.08727	0.707	1.08727	[21]	[18,21]

TABLE II. Values of Coulomb barrier height U_B, radius R_B, and curvature factor $\hbar\omega_B$. The results of fusion radius R_F with those of $r_F = R_F/(A_1^{1/3}+A_2^{1/3})$ bracketed along with the range of energy studied in this paper are listed.

System	$E_{\text{c.m.}}$ range (MeV)	$\hbar\omega_B$ (MeV)	U_B (MeV)	R_B (fm)	$R_F(r_F)$ (fm)
$^{16}O+^{152}Sm$	50–75	4.3	58.6	11.43	11.36(1.44)
$^{16}O+^{154}Sm$	50–75	4.2	58.5	11.46	11.38(1.44)
$^{58}Ni+^{58}Ni$	85–115	3.8	104.5	10.03	10.92(1.41)
$^{58}Ni+^{64}Ni$	85–115	3.7	102.8	10.23	11.21(1.42)
$^{64}Ni+^{64}Ni$	85–115	3.6	101.1	10.42	11.36(1.42)
$^{64}Ni+^{92}Zr$	120–165	3.7	133.4	11.27	11.91(1.40)
$^{64}Ni+^{100}Mo$	125–155	3.6	138.7	11.38	12.22(1.41)

EFB model and the justification of considering $T_C = T_{Rl}P_{Sl}$ in the case of a complex square well potential with a complex rectangular barrier. The following results clearly support the above observations.

(i) Utilizing a common radius R_F in the barrier region, the values of the cross sections from DRM and EFB concepts using T_C are comparable. (ii) The cross section resulting from T_C is found to be similar to that obtained by replacing T_C by the product $T_{Rl}P_{Sl}$. It may be pointed out that the latter result allows one to avoid the use of a complicated complex turning point WKB approach to deal with reactions of heavy nuclei.

Following the mathematical procedure based on the WKB approximation given by Farina [12], we express T_{Rl} for different l's as a function $E_{\text{c.m.}}$ in the subbarrier and above-barrier region of energy in a consistent manner. The difficulty faced in our earlier works [9–11], that $T_{Rl} \approx 0$ for $l \approx l_g$, is overcome in the present analysis. Having accounted for the effect of the imaginary part of the OMP in the peripheral region through the factor P_{Sl}, which utilizes transit time in a real trajectory for its calculation, the fusion cross section σ_F is expressed in terms of $T_{Rl}P_{Sl}$ as a function of $E_{\text{c.m.}}$. In the application of the present formulation, the only parameter to be selected near the barrier is the fusion radius R_F.

We then proceed to analyze the experimental data of σ_F and the corresponding average angular momenta $\langle l \rangle$ with success over a wide range of energy around the Coulomb barrier in the cases of several HI systems considered under three different categories: (i) asymmetric ($^{16}O+^{152,154}Sm$), (ii) symmetric ($^{58,64}Ni+^{58,64}Ni$), and (iii) nearly symmetric ($^{64}Ni+^{92}Zr$ and $^{64}Ni+^{100}Mo$). It is found that, for asymmetric pairs, $R_F \approx R_B$, whereas in the cases of other two types of systems $R_F > R_B$. However, in all the cases, the parameter $r_F \sim 1.4$ fm and it is kept fixed over the whole energy range studied. Our results are compared with those obtained by using the DRM, and the closeness of the values of σ_F along with R_F of one model with the other proves their complementary nature as demonstrated in the model calculations in the first part of the paper.

In conclusion, we may mention that the present formulation is a macroscopic approach based on one-dimensional transmission across a complex potential barrier incorporating explicitly the effect of peripheral processes in the dynamics of the fusion mechanism of heavy nuclei around the Coulomb barrier. The method is very simple to apply by selecting a single radius parameter r_F around the value 1.4 fm for all HI pairs, and this need not be changed for the whole energy range to be studied around the Coulomb barrier. It is strongly correlated to the concept of the DRM. But unlike in the DRM, in this calculation one can avoid the use of the OMP in the inner region where it is not known with certainty. On the other hand, the construction of the effective barrier for this formulation implicitly incorporates the effect of channel couplings. The method is found to show remarkable success in explaining the measured σ_F and $\langle l \rangle$ data simultaneously in several cases of heavy pairs of nuclei. In view of the results of R_F being larger than R_B and exponentially decreasing values of the survival probability factor due to a stronger imaginary potential in the inner region ($r < R_F$), we believe that the mechanism of fusion gets initiated from a point outside the barrier and the two-body picture is lost within a short distance inside the barrier.

ACKNOWLEDGMENTS

One of us (B.S.) gratefully acknowledges research grant No. SP/S2/K14/96 (PRU), DST, New Delhi and the facilities extended to him by Institute of Physics, Bhubaneswar and Nuclear Science Center, New Delhi. Two of us (C.S.S. and I.J.) thank Nuclear Science Center, New Delhi for the research facilities provided to them during their visits.

[1] M. V. Andrés, F. Catara, Ph. Chomaz, and E. G. Lanza, Phys. Rev. C **39**, 99 (1989); J. Phys. G **14**, 1331 (1988).

[2] S. C. Pieper, M. J. Rhoades-Brown, and S. Landowne, Phys. Lett. **162B**, 43 (1985).

[3] A. A. Ioannides and R. S. Mackintosh, Phys. Lett. **161B**, 43 (1985).

[4] A. B. Balantekin, S. E. Koonin, and J. W. Negele, Phys. Rev. C **28**, 1565 (1983).

[5] M. M. Shalaby and G. R. Satchler, Nucl. Phys. **A442**, 469 (1985).
[6] G. Michaud, Phys. Rev. C **8**, 525 (1973); G. Michaud, L. Scherk, and E. Vogt, *ibid.* **1**, 864 (1970).
[7] G. R. Satchler, M. A. Nagarajan, J. S. Lilley, and I. J. Thompson, Ann. Phys. (N.Y.) **178**, 110 (1987).
[8] T. Udagawa, B. T. Kim, and T. Tamura, Phys. Rev. C **32**, 124 (1985).
[9] B. Sahu and C. S. Shastry, J. Phys. G **15**, 1149 (1989).
[10] B. Sahu and C. S. Shastry, J. Phys. G **16**, 55 (1990).
[11] B. Sahu and C. S. Shastry, J. Phys. G **22**, 1483 (1996).
[12] J. E. G. Farina, J. Phys. A **21**, 2547 (1988).
[13] H. D. Marta, R. Donangelo, D. Tomasi, J. O. Fernández Niello, and A. J. Pacheco, Phys. Rev. C **54**, 3156 (1996).
[14] N. Takigawa, M. Kuratani, and S. Yoshida, in *Heavy Ion Reactions with Neutron Rich Beams*, edited by M. Ishihara, N. Takigawa, and S. Yamaji (World Scientific, London, 1993), p. 252.
[15] G. R. Satchler, M. A. Nagarajan, J. S. Lilley, and I. J. Thompson, Phys. Rev. C **41**, 1869 (1990).
[16] R. M. More and K. H. Warren, Ann. Phys. (N.Y.) **207**, 282 (1991).
[17] D. M. Brink, *Semi-Classical Methods for Nucleus-Nucleus Scattering* (Cambridge University Press, London, 1985).
[18] A. M. Stefanini, Nucl. Phys. **A538**, 195c (1992).
[19] T. Izumoto, T. Udagawa, and B. T. Kim, Phys. Rev. C **51**, 761 (1995).
[20] D. Ackermann *et al.*, Nucl. Phys. **A609**, 91 (1996).
[21] M. L. Halbert, J. R. Beene, D. C. Hensley, K. Honkanen, T. M. Semkow, V. Abenante, D. G. Sarantites, and Z. Li, Phys. Rev. C **40**, 2558 (1989).